9th International Conference on Contact Mechanics and Wear of Rail/Wheel Systems
(CM2012), Chengdu, China, August 27-30, 2012

AN INVESTIGATION INTO THE RELATION BETWEEN WHEEL/RAIL CONTACT AND BOLT TIGHTNESS OF RAIL JOINTS USING A DYNAMIC FINITE ELEMENT MODEL

M. Oregui [1)*], Z. Li [1)], and R. Dollevoet [1)]

1) Section of Road and Railway Engineering, Faculty of Civil Engineering and Geosciences, Delft University of Technology

* m.oregui@tudelft.nl

ABSTRACT

Rail joints have a shorter service life than most other railway track components. The discontinuity between rail ends turns the rail joint into a weak spot, and consequently, into a track component demanding more frequent maintenance measures, which result in high maintenance costs. Moreover, difficulties are often found when assessing the damage condition of rail joints since damage conditions like cracks in the rail web or loose bolts cannot be detected by visual inspection. A better understanding of the damage mechanisms and degradation process of rail joints may help to develop adapted maintenance measures and to improve rail joint design. In this paper, a 3D Finite Element model is presented as base for rail joint study. The model represents accurately the main components (rail, sleeper, joint bars and wheel) and the interaction between them (contact). The model is validated between 150 and 800 Hz with measured axle box accelerations of resilient wheels. Higher frequencies may be reached with an improved model of the rubber. In the paper, the influence of the bolt tightness is studied. The results showed that contact force, specially its variation, is strongly affected by the bolt tightness; loose bolts cause higher contact forces. The effect of vehicle speed on wheel/rail contact is also significant mainly due to the interaction between rail and sleepers in the vicinity of the rail joint. Apart from bolt tightness conditions and vehicle speed, the validated model has the potential to study the influence of other track parameters and damage conditions.

1 INTRODUCTION

Rail joints can be found worldwide in railway networks and are used either to connect rails or to isolate track sections for signaling purposes. Since they constitute a discontinuity, rail joints are a weak spot with a short service life in the track structure. Compared to other track elements, more frequent maintenance and renewal actions are needed. The difference between the service life of a continuously welded rail and a rail joint was shown to be a factor of 5 [1]. This directly increases the maintenance costs, and there is the additional challenge of having to define the right time for maintenance and renewal since the damage state of rail joints is difficult to assess; for example, cracks in the rail web or loose bolts cannot be identified by visual inspection.

To gain a better understanding of the fast deterioration of rail joints, studies have been carried out on, among others, the following two aspects: the rail discontinuity and the contact between joint bars and rails. The discontinuity between rails can be empty or filled with an isolating material; in both cases the contact between the wheel and the rail is highly affected by the discontinuity, as Chen and Kuang [2] showed in their static analysis. They used a Finite Element (FE) model without bars where the discontinuity created a non-uniform wheel/rail pressure distribution and high maximum shear stresses. Chen and Kuang also pointed out the need for a 3D FE model to reproduce wheel/rail

contact at rail joints, because the results differed considerably from the Hertzian contact solution. With a 3D FE model, Sandström and Ekberg [3] modeled part of a wheel rolling over two short rails with isolating material in between. Their results are of static or low speed dynamics characteristic owing to the nature of the Abaqus/Standard employed. In line with Chen and Kuang's results, Sandström and Ekberg found that the high contact loads caused a concentration of stresses on rail ends leading to ratcheting on rail ends. Pang and Dhanasekar [1] went a step further in analyzing the effects of the discontinuity under rolling conditions by modeling a whole joint with an explicit integration scheme to account for the high frequency dynamics. Rail, wheel, joint bars and isolating material were represented in 3D while the rail, isolating material and joint bars were modeled as one component, that means no contact was defined between them. The study reaffirmed the significant influence of the discontinuity on the wheel/rail contact. Pang and Dhanasekar showed that not only the pressure distribution, but also the contact patch size and the maximum contact pressure differed from Hertzian solution. Wen et al. [4] extended the dynamic study by analyzing the effect of axle loads and train speed in the joint region. Their model considered the gap as well as the contact between rail and joint bars but the excluded the holes on the rail; the fastening, the sleeper and the ballast were simplified to an equivalent support. They concluded that higher dynamic forces, stresses and strains were obtained when increasing axle load or train speed, but the influence of the speed was weak.

To examine the effect of joint bars for dynamic wheel loads, Li et al. [5] developed a 3D FE model where wheel, rail, joint bars and sleepers were modeled using their real geometry. Neither discontinuity nor isolating material was included, but the contact between the bars and the rail was considered. They observed the importance of bolt tightness in wheel/rail dynamics: loose bolts lead to high dynamic contact force.

So it is established that the rail discontinuity, the bolt tightness and the related contact conditions between joint bars and rail have a substantial influence on the wheel/rail contact, leading to high impact forces, high stress concentration and permanent plastic deformation. However, these phenomena have been studied separately in the literature, while in reality there is interaction; different conditions of joint bar/rail contact may affect the impact loads at the rail ends and consequently the stresses in the contact patch, the rail, the bars, the fastening, the sleepers and the ballast, resulting in deterioration of the rail joint assembly and the local track structure.

In this paper, the combined influence of rail discontinuity and tightness of joint bars on wheel/rail contact and vehicle-track interaction is studied though a finite element method. With an Explicit FE approach, train-wheel/rail-track interaction over a rail joint is simulated in the time domain. The model is validated by Axle Box Acceleration (ABA) measurements. The effect of vehicle speed on the contact force is analyzed. Three bolt tightness conditions are studied to investigate the influence of the bolt tightness on the wheel/rail dynamic contact forces.

Once the model is validated, the next steps of our research will consist of a further study of track parameters and elements so that the degradation mechanism of rail joints can be better understood. Modeling the rail discontinuity, the rail bolt tightness, and other related contact conditions interactively in one integrated model has two benefits. First, it may help to understand the mechanisms and rates of degradation of the components and the assembly under the mutual influence of the discontinuity and the bolt tightness. This may lead to improved rail joint design. Second, it may help to establish quantitative relationships between the characteristic frequencies of damage conditions (also called signature tunes) and degradation severity and rates of the components, so that predictive maintenance can be achieved.

2 MODEL

The model simulates the vehicle-wheel/rail-track interaction over a rail joint (see Figure. 1). The model includes a simplified vehicle and a detailed track where wheel, sleepers, rail and joint bars are modeled with their real 3D geometry using solid elements. Figure 2

shows an overview of the 3D FE model. The gap between the rail ends is included. The BS-80A rail, with 1/40 inclination, is supported by wooden sleepers. The rail model accounts for plastic deformation and kinematic hardening with a bilinear elastoplastic material. The joint bars are of a strengthened type for the BS-80A rail and are considered as being elastic.

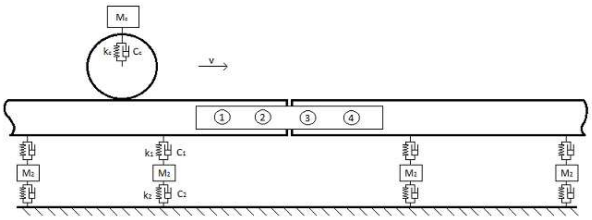

Fig. 1. Schema wheel over rail joint

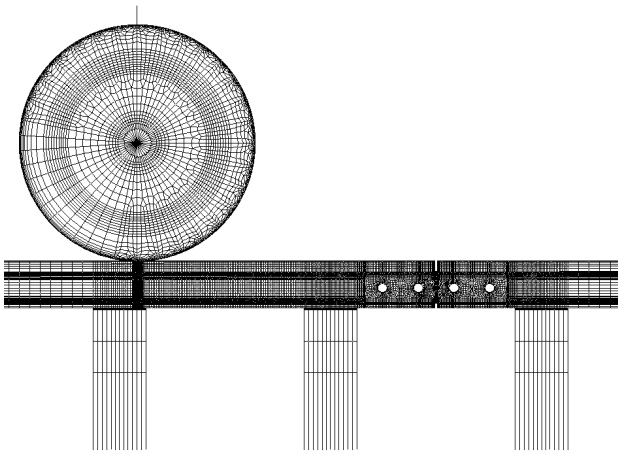

Fig. 2. Overview 3D FE model wheel over rail joint

The wheel diameter is 670 mm. The wheel consists of steel and has a rubber ring between the tire and the web. The steel is modeled elastically for the wheel web and elastoplastically with kinematic hardening for the tire. The rubber is represented as a continuous ring, although in reality it consists of discrete rubber blocks as shown in Figure 3. The rubber is modeled with a Mooney-Rivlin model with damping proportional to the stiffness. The Mooney-Rivlin model requires a curve of an uniaxial test and the dimensions of the test specimen. Compression test data on rubber blocks are available for such purpose. Since the test specimen has to be defined as a rectangular prism in the material model, the rubber block is simplified to a prism of 100 mm length, 50 mm width and 30 mm height. The curve is fitted with the least square method, and this fit is used in the simulation.

Fig. 3. Rubber in the wheel – specimen

Figure 4 shows the average force-deformation curve (the continuous line). When implementing the curve in the model, the working condition of the rubber must be considered because the rubber block is deformed after the mounting and it is prestressed. This means that the initial working condition is not at the origin in Figure 4 but in a preloaded condition indicated with the star. However, it is not possible to define a prestressed material with zero strain for an non-deformed geometry defined by solid elements. An adapted approach is taken to define a curve that reaches the prestress condition with little deformation but that accounts for the physical meaning that a material cannot be prestress without strain, this is, strain and stress are zero in the origin. The best fit is shown with the dashed line in Figure 4. It covers the working range of the rubber which is known to be between 6 and 7.5 mm of the deformation of the rubber block.

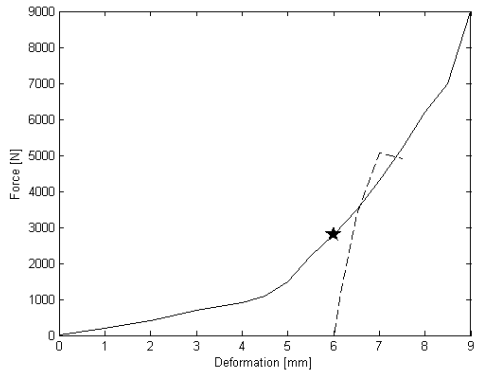

Fig. 4. Uniaxial compression test of the rubber in the wheel (continuous line), best fit to the curve considering rubber's prestress (dashed line) and ★ rubber's initial working condition

The fastening assembly and the ballast are represented by linear springs and viscous dampers in parallel. The vehicle is represented by a single wheel with the sprung mass being lumped together and connected to the wheel with the primary suspension. This assumption is reasonable because of the high frequencies of the studied phenomena.

The bolts are modeled by applying pretension to the hole edge of joint bars. Bolt tightness is calculated according to [4]:

$$P_b = \frac{T}{DK} \quad (1)$$

Where P_b is bolt pretension, T the bolt torque moment, D the bolt diameter and K the coefficient of the bolt torque moment which has values between 0.19 and 0.25 depending on the interface condition. In the current case, it was assumed that the interface and lubricant were perfectly clean (K=0.19) since the studied fish plate was mounted on the location one week before the field test.

With this vehicle/track system modeling, all relevant elements are considered with focus on the accurate modeling of the most influential elements and their interaction. For wheel/rail rolling contact as well as for joint bar/rail contact, surface-to-surface contact is defined with Coulomb friction. The model parameters are summarized in Table 1.

Table 1. Vehicle, track and material data

Component	Parameter	[]	Values
Sprung mass	Mass	kg	3250
First suspension	Stiffness	MN/m	1
	Damping	Ns/m	1122
Fastening	Stiffness	MN/m	1.3
	Damping	kNs/m	33.75
Sleeper	Young’s modulus	GPa	16.6
	Poisson’s ratio	-	0.3
	Density	kg/m^3	1100
	Spacing	m	0.6
Ballast	Stiffness	MN/m	45
	Damping	kNs/m	32
Wheel and rail	Young’s modulus	GPa	210
material (steel)	Poisson’s ratio		0.3
	Density	kg/m^3	7800
	Yield stress	GPa	1.12
Wheel material	Poisson’s ratio		0.49
(rubber)	Density	kg/m^3	1190
	Rayleigh damping		0.01
Bolt tightness	Bolt torque moment	Nm	270
	Bolt diameter	m	0.027
	Bolt torque moment coefficient	-	0.19

3 VALIDATION

3.1 Field test

A field test was performed in Sheffield, UK on the Supertram network in August, 2011. An Axle Box Acceleration (ABA) measuring system was installed on a regular tram which run on a track section so that the vertical acceleration of the axle box was measured. The studied track section contained a number of fish-plated joints (FP), among them, the reference FP is shown in Figure 5. Rail vertical profiles at the reference FP were also measured to be used later in the FE model.

Fig. 5. Reference FP on the Supertram tram network, Sheffield

3.2 Model validation

The strength of the ABA measurement system is based on the analysis of the impact response of the axle due to irregularities or anomalies. Therefore, the study was focused on the signal analysis at and after the rail gap.

The signal was band pass filtered between 150 and 1500 Hz. The low frequency limit was necessary to make the high frequency behavior noticeable while at very high frequency no relevant energy concentrations were observed. Figure 6 shows the wavelet power spectrum diagram of the measurement. Most of the energy is concentrated between the beginning of the gap at 0.847m and the bolt at 0.9 m. The dominant frequency range covers between 150 and 500 Hz, although there is a relevant energy concentration around 1000 Hz immediately after the gap. No energy concentration is noticed around the bolt at 1.0 m or at the end of the FP at 1.05 m.

The wavelet power spectrum diagram of the simulation is shown in Figure 7. Compared to the measurement, one can see that the simulation is able to reproduce the energy distribution regarding both frequency

components and space distribution in the dominant frequency range 150-500 Hz. Although less prominent than in the measurement, a subtle energy concentration is noticed at high frequency around the gap. Unlike the measurement, the simulation shows a noticeable energy concentration around 1.07 m. At this location, a sleeper starts and rail/sleeper interaction results, this phenomenon is further studied in the following section.

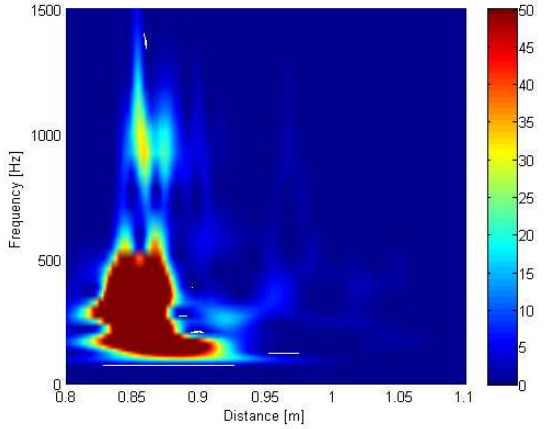

Fig. 6. Wavelet power spectrum: measured ABA at reference FP. The 6 mm gap begins at 0.847 m

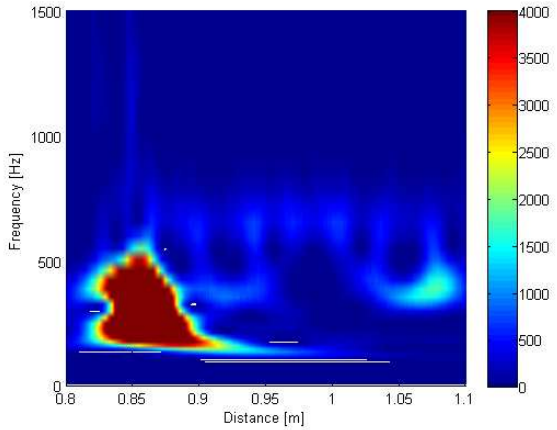

Fig. 7. Wavelet power spectrum: simulated ABA

The fact that the model gives an accurate reproduction of one frequency range while another is only roughly approximated may be related to the material model of the rubber of the wheel. Rubber damping is defined as a constant value proportional to the stiffness. This approach may be accurate for the frequency range 150-500 Hz, but frequency independent values may not be adequate to cover the whole frequency range of interest 150-1500 Hz. For railpad modeling, studies showed that frequency dependency should be considered [6]. Therefore, frequency dependency will be studied in future work.

The dominant frequency and location of the energy concentration were reproduced numerically, but the energy magnitudes were not. The simulated ABA have higher energy values than the measured one. This may be explained when both signals are compared in the time domain, see Figure 9. One can see that the simulated acceleration is higher than the measured one and that the simulation does not die out completely. This may also be related to the material model of the rubber of the wheel. Static test values were used for the material definition while, at least in the case of railpad modeling, studies showed that dynamic values should be used [7]. An improvement of the rubber modeling will be considered in the future steps where including the dynamic behavior and/or the frequency dependency will be studied.

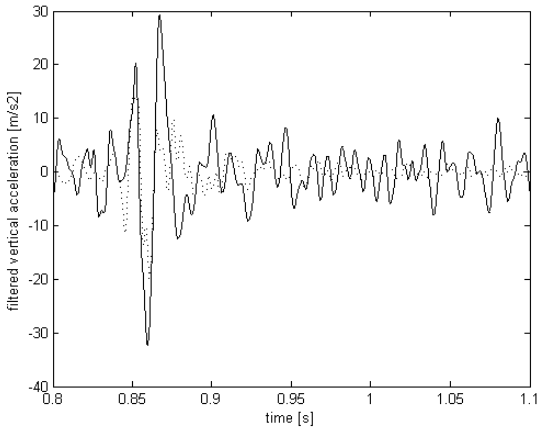

Fig. 9. Measured (…) and simulated (-) signal in the time domain (filtered signals between 150 and 3000 Hz)

4 NUMERICAL RESULTS

4.1 Effect of train speed

The influence of the vehicle speed on the contact force has been studied. The analysis shows a strong effect of the vehicle speed on the contact force: the faster the vehicle, the higher the largest contact forces (see Figure 10). This result differ from Wen et al. who concluded that the effect of train speed is relatively weak [4]. However, there are two main differences

between Wen et al.'s model and the one presented in this paper.

First, this model includes measured rail vertical geometry, unlike Wen et al.'s model which used smooth running surfaces. The measured geometry shows misalignment between the rail ends (see Figure 11) which leads to an impact between the wheel and the rail when the wheel runs over the discontinuity. At higher vehicle speed, higher impact is expected.

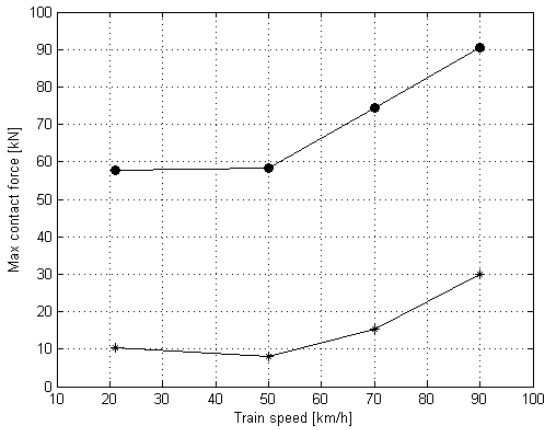

Fig. 10. Largest vertical contact forces vs. speed: • wheel/rail contact, *rail/sleeper contact

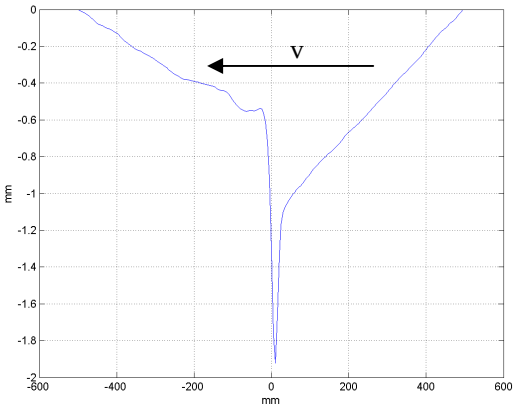

Fig. 11. Measured rail vertical geometry at reference FP

The second difference lies with the track element representation. Wen et al. simplified the fastening system, the sleeper and the ballast to an equivalent vertical support. The presented model, however, represents the sleeper with 3D solid elements and the fastening system and the ballast with springs and dampers. Moreover, contact between rail and sleepers close to the FP structure is defined. The analysis of these contacts shows that rail/sleeper impact takes place when the wheel runs over the gap. In Figure 10, one can see that between 21 (the measured vehicle speed) and 50 km/h, the largest wheel/rail contact forces increases only slightly with speed, while rail/sleeper impact contact does not increase. However, between 50 and 90 km/h, the largest wheel/rail contact forces increase considerably, resulting in an increase in rail/sleeper contact forces. The different behavior in the two vehicle speed ranges will be further studied.

4.2 Effect of bolt tightness condition

Figure 12 shows the contact force between wheel and rail for three bolt tightness conditions. In the first case, called *nominal*, the torque applied to the bolts to tighten them is 270 Nm. In the second case, which is indicated as *loosen*, the torque of all four bolts is reduced to 150 Nm. In the third case, the first two bolts are completely loose (i.e. torque is 0 Nm) while the last two are tightened with a torque of 150 Nm. This last case is called *half-loose*.

One can see that the largest contact force is higher for conditions with loose bolts than for the nominal condition, although no trend is found related to the degree of tightness. The contact force oscillation, however, shows a trend: the biggest variation is reached at the loosest case (*half-loose*) and the smallest at the *nominal* case, which is in agreement with Li et al [5].

Li at al. also concluded that completely loose bolts considerably affected the contact force while half-loosen bolts did not. With the current FE model, however, one can see that the contact force reaches higher largest and variation values than in the *nominal* condition not only in the *half-loose* condition but also in the *loosen* condition. Furthermore, by comparing the wavelet diagrams (see Figure 7 for the *nominal* case, Figure 13 for the *loosen* case and Figure 14 for the *half-loose* case), one can see that the most significant difference is between the *nominal* case and the cases with loose bolts. The peak in energy distribution around 400 Hz covers a longer distance in the *loosen* and *half-loose* conditions (up to 0.97m) than in the *nominal* one (up to 0.91m), with the *half-loose* case having the highest energy

concentration at this frequency. Apart from the amount of energy, almost no difference is noticed between *loosen* and *half-loose* conditions. One should be aware that the analyzed signals cover from the gap to the end of the fish plate where both *loosen* and *half-loose* conditions share the same bolt tightness condition (i.e. a torque of 150Nm is applied to the two bolts in the analyzed FP half). A study of the signal of the whole FP may reveal differences that are not noticed in this analysis.

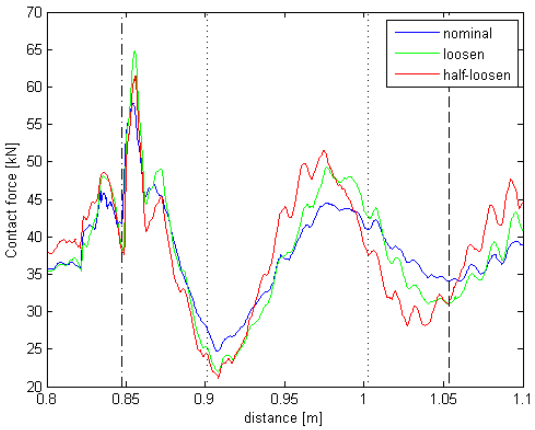

Fig. 12. Wheel-rail contact force for three bolt tightness conditions. Vertical lines: -. gap begin, .. bolt location and -- fish plate end.

The difference between Li et al.'s and the present results may be explained by analyzing the effect of the gap which is included in the presented model whereas Li et al. modeled a continuous rail. Structurally, the gap makes the rail joint more flexible. Moreover, the bolt tightness conditions are different. In this paper, the torque of all four bolts is decreased which leads to a more flexible structure instead of having only two loosened bolts as in Li et al.'s paper. The increased flexibility changes the stiffness of the track so that the effect is noticed on wheel/rail interaction. Dynamically, the gap causes an impact between wheel and rail. While Li et al. ignored the influence of the gap to concentrate on and highlight the effect of stiffness change at the fish plate end, in the present model, the impact contact force is clearly the dominant peak. The impact together with the extra flexibility determine rail joint behavior so that higher differences are reached between the largest and the smallest contact force (from now on called contact force variations) in bolt tightness conditions where Li et al.'s model gave low variations. This shows that there is interaction between discontinuity and the FP structure and that both gap and rail/joint bar contact should be considered when studying the rail joint behavior. This is because the high contact force variation can lead to differential wear and differential plastic deformation which will, under certain conditions, result in permanent deformation [5].

The comparison of the three bolt conditions also shows a difference in energy concentration between 1.05 and 1.1m (see Figure 7 for the *nominal* case, Figure 13 for the *loosen* case and Figure 14 for the *half-loose* case). This is reflected in the wheel/rail contact forces where higher values are reached as shown in Figure 12. This phenomenon is related to the rail/sleeper contact; the looser the bolts, the higher the contact force between rail and sleeper.

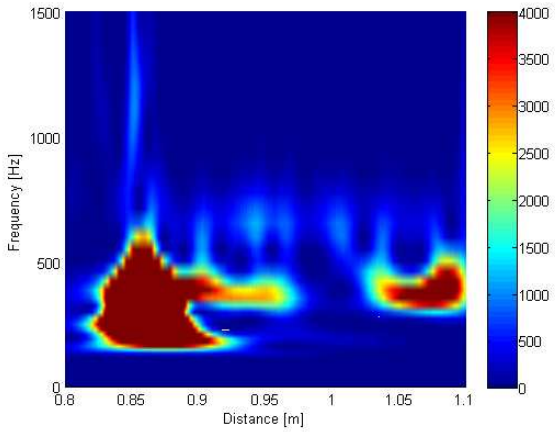

Fig. 13. Wavelet power spectrum: *loosen* bolt tightness condition

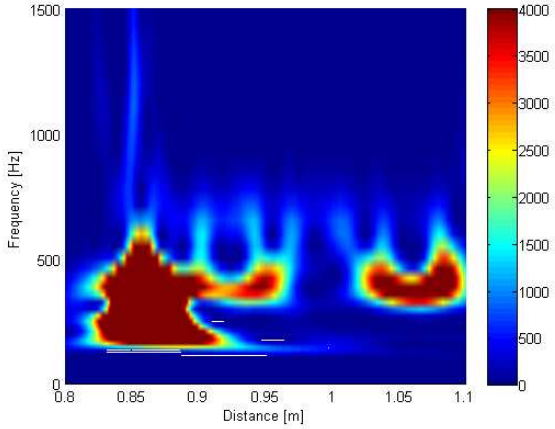

Fig. 14. Wavelet power spectrum: *half-loose* bolt tightness condition

Although the study about bolt tightness conditions is not yet complete, this first analysis gives an insight into the effect of bolt tightness condition on wheel/rail contact forces. The increased energy concentration around 400 Hz may be useful information for the development of preventive maintenance since it could be applied to detect loose bolts.

5 CONCLUSIONS

A 3D Finite Element model has been presented for the study of fish-plate joints where the model accounts for the resilient component of the wheel and the contact between the main components of the structure (wheel, rail and joint bars). The response of a wheel running over a FP was reproduced and validated in the frequency range 150-800 Hz by axle box acceleration measured on resilient wheels. For higher frequencies, an improved model of the rubber ring in the wheel needs to be considered. With the validated model, two studies were carried out.

First, the effect of vehicle speed on the contact between wheel and rail was studied. The strong influence of speed is directly related to (1) the rail end geometry; rail end misalignment leads to higher impact loads at higher speeds (2) rail/sleeper contact in the vicinity of the FP structure; the higher the impact contact between wheel and rail, the higher the contact forces between rail and sleeper. This shows that contact between rail and sleeper needs to be considered to properly reproduce the track behavior close to a rail joint.

The second study analyzed the influence of bolt tightness condition on wheel/rail contact. Two main conclusions were drawn. First, a FP with partly or completely loose bolts gives rise to higher largest contact force between wheel and rail than the nominal bolt tightness condition. Second, the loosening of the bolts increases the contact force variation which may lead to differential wear and differential plastic deformation. This may result in permanent deformation, if the force variation is always at the same location and with the proper wavelength.

The presented studies gave a first insight into structural behavior and wheel/track interaction at a rail joint. The validated model is the base for a wide and complete study.

ACKNOWLEDGEMENTS

The project has been partly financed by the EC-funded FP7 PMnIDEA project. We are grateful to Rob Carrol, Supertram –Stagecoach, Shefield. The first author was supported by the Basque Government of Spain with grant BFI10.

REFERENCES

[1] T. Pang and M. Dhanasekar, Dynamic finite element analysis of the wheel-rail interaction adjacent to rail insulated rail joints, presented at the 1th International Conference on Contact Mechanics and Wear of Wheel/rail Systems, 2006.

[2] Y. C. Chen and J. H. Kuang, Contact stress variations near the insulated rail joints, Proceedings of the Institution of Mechanical Engineers, Part F: Journal of Rail and Rapid Transit, 216 (2002) 265-274.

[3] J. Sandström and A. Ekberg, Numerical study of the mechanical deterioration of insulated rail joints, Proceedings of the Institution of Mechanical Engineers, Part F: Journal of Rail and Rapid Transit, 223 (2009) 265-273.

[4] Z. Wen, et al., Contact-impact stress analysis of rail joint region using the dynamic finite element method, Wear, 258 (2005) 1301-1309.

[5] Z. Li, et al., Differential wear and plastic deformation as causes of squat at track local stiffness change combined with other track short defects, Vehicle System Dynamics, 46 (2008) 237-246.

[6] Y. Sato, Study on high-frequency vibrations in track operated with high-speed trains, Quarterly Report of RTRI (Railway Technical Research Institute) (Japan), 18 (1977) 109-114.

[7] D. J. Thompson, et al., Developments of the indirect method for measuring the high frequency dynamic stiffness of resilient elements, Journal of Sound and Vibration, 213 (1998) 169-188.